Suppression of Oscillator Bias Voltage Phase Noise via MEMS Resonator Arraying

Jeffrey Ni

Electrical Engineering and Computer Sciences
University of California, Berkeley

Technical Report No. UCB/EECS-2022-119
http://www2.eecs.berkeley.edu/Pubs/TechRpts/2022/EECS-2022-119.html

May 13, 2022

Suppression of Oscillator Bias Voltage Phase Noise via MEMS Resonator Arraying

by Jeffrey Ni

Research Project

Submitted to the Department of Electrical Engineering and Computer Sciences, University of California at Berkeley, in partial satisfaction of the requirements for the degree of **Master of Science, Plan II**.

Approval for the Report and Comprehensive Examination:

Committee:

Professor Clark Nguyen
Research Advisor

5/13/22

(Date)

* * * * * * *

Professor Kris Pister
Second Reader

5/13/22

(Date)

Suppression of Oscillator Bias Voltage Phase Noise via MEMS Resonator Arraying

by

Jeffrey Ni

A dissertation submitted in partial satisfaction of the

requirements for the degree of

Master of Science

in

Electrical Engineering

in the

Graduate Division

of the

University of California, Berkeley

Committee in charge:

Professor Clark Nguyen, Chair
Professor Kris Pister

Spring 2022

Suppression of Oscillator Bias Voltage Phase Noise via MEMS Resonator Arraying

Abstract

Suppression of Oscillator Bias Voltage Phase Noise via MEMS Resonator Arraying

by

Jeffrey Ni

Master of Science in Electrical Engineering

University of California, Berkeley

Professor Clark Nguyen, Chair

Microelectromechanical system (MEMS)-based oscillators are in the heart of many of our electronic devices today, forming the timing basis for our increasingly higher frequency circuits. High-performance, low-noise oscillators are critical to meeting the standards of today's communication protocols. Effects of noise from all inputs of a circuit to the final output spectrum should be understood to make better oscillators, and this report specifically considers the effects of noise on the bias voltage supply needed for strong electromechanical coupling to sustain resonance. We investigate how arraying multiple MEMS resonators—putting multiple copies of the same resonant structures in parallel and mechanically coupling them so they resonate together—for use in an oscillator can potentially lead to better resilience against phase noise induced by this source of noise compared to a single resonator.

We set out to first measure the sensitivity of high-Q wineglass-disk-based MEMS oscillators to bias voltage noise to determine which types of noise (noise from direct mixing versus noise from resonant frequency modulation) dominate at which frequency regimes. This establishes a baseline that we can compare against prior work in this area done on a different resonator structure. Then we construct oscillators around different sized arrays to determine the effects of arrays on this sensitivity and see if they can provide better noise performance.

We show how there is improved close-to-carrier phase noise performance at the cost of potentially increased power consumption due to increased loading capacitance for an array compared to a single-device-based oscillator. Without increasing the power, measurements show degraded far-from-carrier noise rejection for arrays due to lower output oscillation level.

To my family.

Contents

List of Figures

List of Tables

Acknowledgments

I would like to thank Qianyi Xie for helping me with releasing the devices and getting started with the measurements for this project and Kevin Zheng for helping me out with problems I ran into during my time in the group and reading my drafts of this work. I also express thanks to Prof. Kris Pister for being the second reader for this thesis. Finally, I'd like to thank Prof. Clark Nguyen for taking me into his lab several years ago and being my advisor.

Chapter 1

Introduction

Microelectromechanical system (MEMS)-based resonators and oscillators are ubiquitous in our everyday electronics to provide precise frequency and timing information. They are able to provide equal or better frequency stability than conventional crystal based oscillators and also have found use in other applications such as filters and sensors. These resonators require high enough DC bias voltages to maintain sufficiently large electromechanical coupling to sustain oscillation — just above current I/O voltages for the latest small gap devices [1]. Noise from adjacent switching digital circuits on the same supply or coupled in from the resonator's ports will show up on the bias voltage and be upconverted to spurs around the oscillation frequency via a combination of frequency modulation and direct voltage noise, affecting the performance of the oscillator.

The effects of these noise sources has been documented before [2] on a double-ended tuning fork MEMS resonator structure. They show how close-to-carrier noise is dominated by frequency modulation induced noise and far from carrier voltage amplitude noise takes over. Prior work [3] has also shown how arraying resonators in parallel can reduce the variability of the resonant frequency from changes in the bias voltage via a reduction in the effect of the negative electrical stiffness. This means that for the same amplitude noise on the bias voltage, one should expect less frequency modulation with larger arrays. To build upon these ideas, we investigate how arrayed MEMS resonators can lead to smaller noise spurs in the close to carrier FM-dominated frequency regime and better phase noise performance. Using different sized arrays of 61MHz wine-glass mode disk devices, we first characterize the resonant frequency vs bias voltage of the different arrays outside of an oscillator. We then measure their phase noise and output spectrum in an oscillator circuit.

Chapter 2

Theory

2.1 MEMS Resonator Frequency Stability Review

For MEMS resonators where the direction of vibratory motion is perpendicular to the faces of the capacitor that generates the gap closing force, there is a well-documented effect where as the bias voltage on the body of the resonator increases, the resonant frequency of the structure decreases. This is due to an equivalent electrical stiffness k_e that increases with voltage, and to a first order approximation it is like a spring with a negative spring constant. The stiffness is generated by the changing electric fields between the resonator body and the electrodes as the gap between them expands and contracts during resonance. The linear term of this stiffness is given by the expression (2.1) [4].

$$k_e = \frac{V_P^2 \epsilon A}{d_0^3} \tag{2.1}$$

Shifts in frequency due to this electrical stiffness can impact the stability of MEMS-based oscillators, and prior work [3] [5] has shown theoretically and experimentally how resonators mechanically linked in arrays can have less sensitivity to changes in their bias voltages. Figure 2.1 compares the potential shift in frequency vs the bias voltage V_P for two different sized resonator arrays. Over the entire V_P span, the 5 disk array has less total shift in resonant frequency than the 1 disk array, and as a result the frequency shift per volt or slope of the plot at the same bias condition is less for the 5 disk array than the 1 disk array.

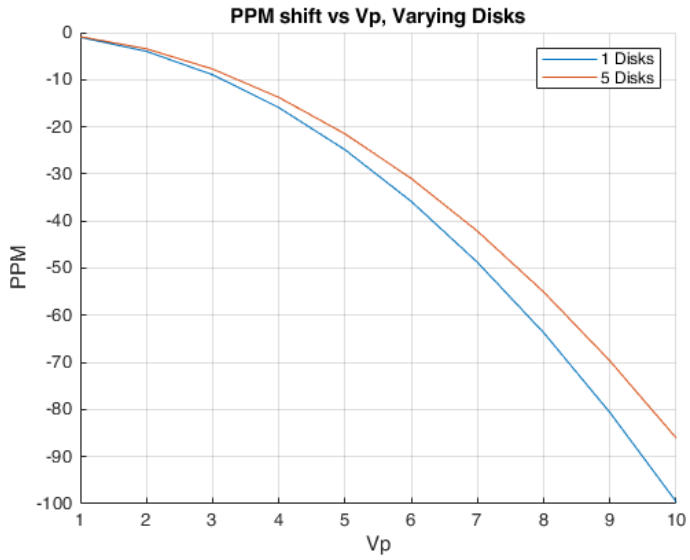

Figure 2.1: Theoretical 1 disk vs 5 disk resonant frequency shift vs V_P with $10k\Omega$ termination resistance.

This improvement in stability can be explained by looking at these mechanical structure from a circuits perspective. An equivalent circuit model of the resonator can be generated from the mechanical parameters of the circuit [5] where m_m is the effective mass, k_m is the effective stiffness at zero bias voltage, and b_m is the effective damping of the structure. The electrical stiffness generates a force in the direction of displacement and is modelled as negative capacitance. The effective negative capacitance from the linear portion of the electrical stiffness is equal to the electrode overlap capacitance after reflecting it across the transformers that model the coupling factor η. η is a a bias voltage-dependent coupling factor that converts the voltage to a force and vice-versa. Putting this all together allows one to use conventional circuit analysis techniques to analyze this problem.

$$l_m = m_m, c_m = \frac{1}{k_m}, r_m = b_m, \eta = V_P \frac{\partial C}{\partial z} \tag{2.2}$$

$$L_m = \frac{l_m}{\eta^2}, C_m = \eta^2 c_m, R_m = \frac{r_m}{\eta^2} \tag{2.3}$$

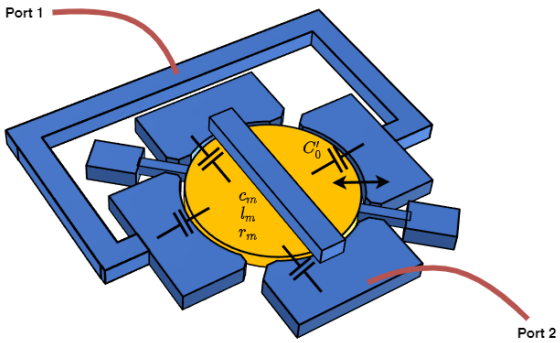

Figure 2.2: Model of a single disk array resonator.

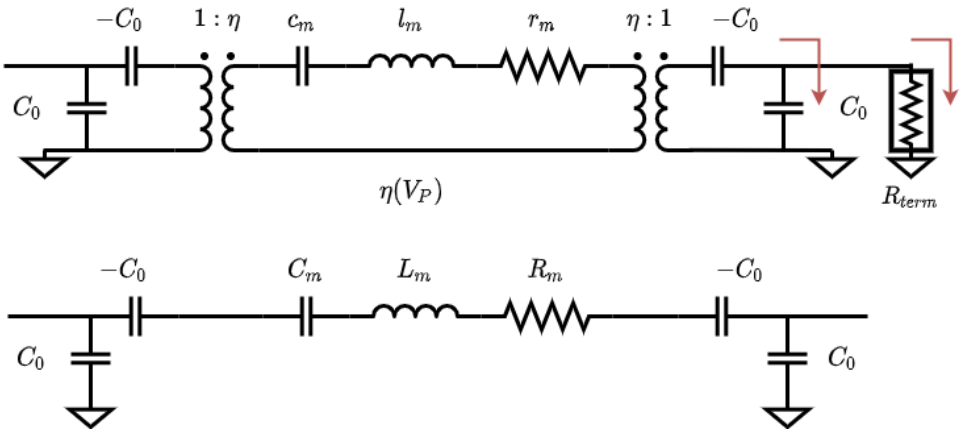

Figure 2.3: Equivalent electrical circuit of the resonator. C_0 is the total capacitance on each port from connected electrodes. The red arrows represent the division of current through the overlap capacitance (which causes the cancellation) and the termination resistance.

Using this circuit model and temporarily disregarding the loading capacitance C_0, the series resonant frequency of the resonator is given by Equation (2.4) [5].

$$f = f_{nom}\sqrt{1 - \frac{C_m}{C_0}} \tag{2.4}$$

$$\approx f_{nom}(1 - \frac{C_m}{2C_0}) \tag{2.5}$$

$$p_{c,\text{unloaded}} \triangleq \frac{f - f_m}{f_m} = -\frac{C_m}{2C_0} \tag{2.6}$$

While the negative capacitance can be useful for tuning of the resonant frequency of the device, it is detrimental to the stability of an oscillator. The instability can be reduced by the cancellation of the negative capacitance effect documented in [3] and is achieved through the diversion of motional current through the overlap capacitance instead of the output port with resistance R_{term}, as illustrated in 2.3. When more current passes through the real overlap capacitance C_0, part of the negative capacitance causing the shift in resonant frequency is cancelled.

The amount of cancellation is a function of the size of the capacitance and the termination resistance. The higher the resistance and capacitance, the greater the cancellation but at the cost of greater load to the sustaining circuit. With the cancellation current going to ground through the capacitor and being lost, the sustaining amplifier will need to use more power; [6] derives the critical G_M needed by a Pierce oscillator to sustain oscillation as Equation (2.7) where the capacitances are labeled in Figure 2.6. C_0 is assumed to the the dominant capacitance in the lumped element C_1 in the figure. The greater C_0 is, the more G_m and power is needed.

$$G_{mcrit0} \cong \frac{\omega}{QC_m}(C_0 + 2C_3)^2 \tag{2.7}$$

2.2 Arrayed resonators

By having multiple disks mechanically coupled together with $\lambda/2$ length beams, they will resonate in-phase and act in parallel [7]. The effective mass, damping, and spring stiffness will be increased by N times but the coupling factor will be increased by a factor of N^2, giving a net change of R_m and L_m decreasing by a factor of N and C_m increasing by a factor of N. See Table 2.1 and Figure 2.4 for a summary of these parameters and the change in the equivalent circuit. C_0 will also increase by a factor of N, which is the main driving factor [3] behind the increased stability. Equation 2.4 alone would show that there is no improved pulling performance without this C_0 for arraying resonators as both C_m and C_0 would increase together. For the cancellation of the effective negative C_0 with the physical C_0 to be effective one also needs to have minimal parasitic capacitance that could decrease the impedance seen looking out of the resonator, as visualized in Figure 2.5.

Single Disk			**N Disk Array**		
Mechanical Element	Circuit Element		Mechanical Element	Circuit Element	
m_m	l_m	L_m	Nm_m	Nl_m	L_m/N
k_m	c_m	C_m	Nk_m	c_m/N	NC_m
b_m	r_m	R_m	Nb_m	Nr_m	R_m/N
-	-	C_0	-	-	NC_0

Table 2.1: Summary of how the mechanical and circuit parameters change with arrays.

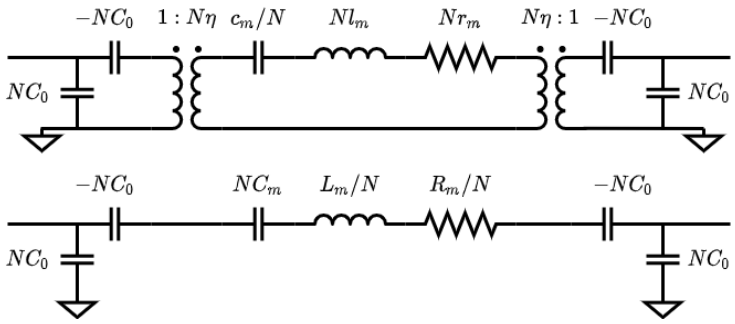

Figure 2.4: Equivalent circuit of N-arrayed resonators.

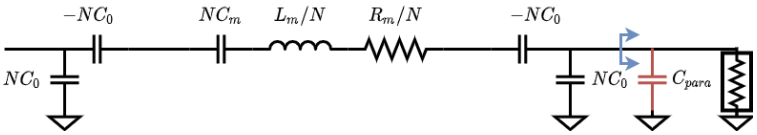

Figure 2.5: Parasitic capacitance affecting the output impedance.

At the same bias voltage, an array N times larger will have all capacitances in Equation 2.7 for the G_M increase by N, meaning the G_m required will also scale with N.

To try to maintain equal operating conditions for all array sizes, the V_P should be adjusted accordingly to give the same motional resistance. This will in turn mean that we need to adjust the Pierce oscillator circuit to match the new power requirements; decreasing V_P to match this resistance will decrease C_m and further scale up the G_m required.

There may also be some second-order effects of increased bypass capacitance on the voltage bias from the greater number of disks and their overlap capacitance, but this should be negligible compared to the parasitic capacitance on the die and the decoupling from the power supply and bias tee.

2.3 Oscillator Frequency Pulling: Frequency Modulation Noise

Multi-resonator arrayed oscillators primarily aim to reduce phase noise that arises from the modulation of electrical stiffness by bias voltage fluctuations, which in turn modulates the resonant frequency.

While in oscillation, the Pierce oscillator does not resonate perfectly at the resonant frequency of the MEMS resonator. Part of the shift is due to additional frequency pulling from load and parasitic capacitances. The amount of pulling in the lossless case is given by

Equation (2.8) [6] and is the effect that is observed with arrayed resonators [3], where C_m is the motional capacitance of the resonator, C_s is the series combination of C_1 and C_2 in Figure 2.6, and C_3 is the capacitance in parallel with the resonator:

$$p_c \approx \frac{C_m}{2(C_s + C_3)} \tag{2.8}$$

For our MEMS resonator, C_m is a series combination of the effective negative capacitance formed by electrical stiffness and the actual motional capacitance of the main resonant structure. With noise on the bias voltage of the structure changing the amount of electromechanical coupling and the electrical stiffness, the C_m is now time-dependent. For an array with N resonators, the load capacitance $C_s = C_0/2$ (assuming that C_0 dominates over other capacitances at the node) and the motional capacitance will both increase by N, generally increasing the static amount of pulling.

$$p_c(t) = \frac{C_m(t)}{2(C_s + C_3)} \tag{2.9}$$

$$= \frac{c_x N[\eta(t)]^2 || - NC_0}{2(\frac{N}{2}C_0 + C_3)} \tag{2.10}$$

$$= \frac{N(c_x V_P(t)^2[\frac{\partial C}{\partial z}]^2 || - C_0)}{2(\frac{N}{2}C_0 + C_3)} \tag{2.11}$$

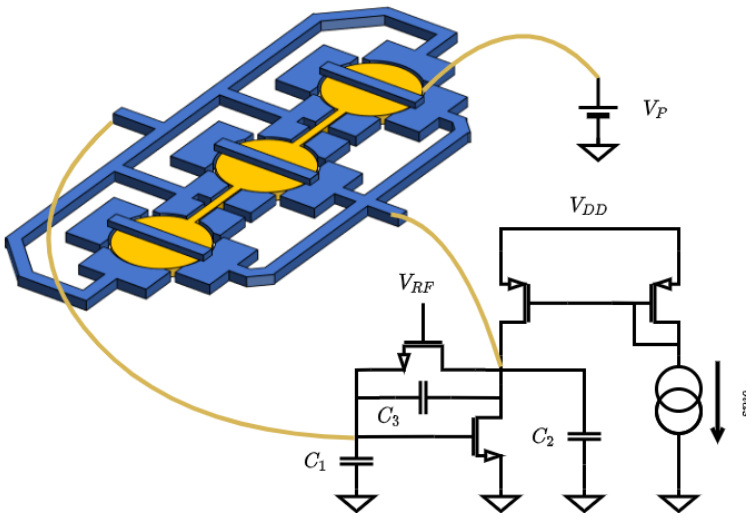

Figure 2.6: Array and Pierce oscillator circuit.

To find the sensitivity to voltage noise we can take the derivative $\frac{\partial p}{\partial V}$ and assume a small perturbation about the operating point. This predicts larger disk arrays to perform worse

than small arrays if driven at the *same bias voltage* and if all capacitances scale with N or if there is no C_3, but improved if driven at the same motional resistance where V_P on a N disk array is $\sqrt{N}$ times smaller regardless of the value of C_3. But C_3 also increases with N as the array becomes physically larger, which also improves the pulling stability but at the cost of power. This increase in C_3 is partially depdendent on layout and a low impedance voltage source for the bias voltage for feedthrough prevention.

For real measurements we can extract the sensitivity of the resonator to the noise from the measured resonant frequency vs V_P curve in Figure 2.1. We linearize the frequency vs voltage dependence around our bias point and calculate the expected amount of modulation and spur level. For example, because the five disk array in Figure 2.1 has less deviation per volt than the single disk array, it should have a lower noise level for a set amount of frequency modulation.

The changing resonant frequency can be modeled as a FM modulator, and when applying a known noise source we can calculate the expected spur levels. A sinusoidal noise source at frequency ω_n creating a deviation of $\pm\Delta\omega$ around ω_c will have levels given by Bessel functions of the first kind . For small arguments like the small noise perturbation in our analysis the Bessel function $J_1(\beta)$ can be approximated as $\beta/2$.

FM modulation with a sinusoidal signal in equation 2.12 can be decomposed into the form of Equation (2.14) with infinite harmonics, but we only consider the frequency components directly adjacent to the oscillator's main oscillation frequency ω_c.

$$w_i(t) = w_c + \Delta\omega\cos(w_n t) \tag{2.12}$$

$$\beta = \frac{\Delta\omega}{\omega_c} \tag{2.13}$$

$$v(t) = \sum_{n=-\infty}^{\infty} J_n(\beta)\cos(w_c + nw_n)t \tag{2.14}$$

$$L(\pm f_{noise}) = 20\log\left(\frac{\mp a v_{noise}}{2f_c}\right) \tag{2.15}$$

$$= 20\log\left(\left|\frac{\mp\beta}{2}\right|\right) \tag{2.16}$$

This simple model assumes that there is no bandwidth limit on the FM modulation of the oscillator. Note that the upper sideband noise has the opposite phase of the input sinusoid. This is important as it will subtract from the in-phase noise contributed by direct voltage noise explained in the next section. As a result one would expect the higher frequency sideband to be lower in level than the lower frequency where the noise adds.

2.4 Direct Voltage Noise

The second noise path is through the mixing of the oscillator's main output signal with the noise through the squaring of the voltage across the capacitive gap by the electromechanical coupling. While detrimental to the performance of the oscillator, this is also the mode that the "mixler" [8] mixer/filter uses to get RF to IF conversion and has been analyzed extensively before. Using prior analysis from that work, one can write the force on the disk as Equation (2.17) with ω_{RF} being the main resonant frequency and ω_n being the noise frequency. Only the terms at the main resonant frequency and the sideband frequencies are expanded out:

$$F = \frac{1}{2}(V_P + v_n \cos(\omega_n t) + v_{RF} \cos(\omega_{RF} t))^2 \frac{\partial C}{\partial z} \tag{2.17}$$

$$= \left(...V_P v_{RF} \cos(\omega_{RF} t) + \frac{1}{2} v_n v_{RF} \cos((\omega_{RF} \pm \omega_n)t)... \right) \frac{\partial C}{\partial z} \tag{2.18}$$

The current coming out of the output electrodes will be where in (2.20) Θ is the transfer function from force to displacement for the given resonator and will take on the form of a bandpass biquad.

$$i = V_P \frac{\partial C}{\partial z} \frac{\partial z}{\partial t} \tag{2.19}$$

$$z = \frac{F}{k} \Theta(j\omega) \tag{2.20}$$

$$\Theta(s) = \frac{\frac{w_0}{Q} s}{s^2 + \frac{w_0}{Q} s + w_0^2}$$

Plugging the forces into the current equations, we get:

$$i_{\omega_{RF} \pm \omega_n} = \frac{1}{2} V_P v_n v_{RF} \left(\frac{\partial C}{\partial z} \right)^2 \frac{\Theta(j(\omega_{RF} \pm \omega_n))}{k} (\omega_{RF} \pm \omega_n) \tag{2.21}$$

$$i_{\omega_{RF}} = V_P^2 v_{RF} \left(\frac{\partial C}{\partial z} \right)^2 \frac{\Theta(j\omega_{RF})}{k} (\omega_{RF}) \tag{2.22}$$

$$\tag{2.23}$$

Taking the ratio of the currents to find the relative noise level, we get Equation (2.24). For small offsets the middle term can be simplified to 1:

$$\frac{i_{\omega_{RF} \pm \omega_n}}{i_{\omega_{RF}}} = \frac{v_n}{2V_P} \left(\frac{\omega_{RF} \pm \omega_n}{\omega_{RF}} \right) \frac{\Theta(j(\omega_{RF} \pm \omega_n))}{\Theta(j\omega_{RF})} \tag{2.24}$$

$$\approx \frac{v_n}{2V_P} \frac{\Theta(j(\omega_{RF} \pm \omega_n))}{\Theta(j\omega_{RF})} \tag{2.25}$$

Given the high-Q performance of the MEMS resonators, Θ will be a very narrowband filter and one can expect to see a decreasing trend in noise level as the noise frequency increases. The predicted noise should not increase with the number of disks, since currents at both the resonant frequency and the spurs gain an increase in output current from the increase in area. We should also see that the higher frequency sideband will have lower levels compared to the lower frequency one due to the parallel resonance of the resonator being higher than the series resonance and making the peak asymmetric.

$$L(\pm f_{noise}) = 20 \log \left(\frac{v_n}{2V_P} \frac{\Theta(j2\pi(f_{RF} \pm f_n))}{\Theta(j2\pi f_{RF})} \right) \tag{2.26}$$

Chapter 3

Experiment

3.1 Setup

The 61MHz wine-glass polysilicon disks were designed in a previous process [9] and released via a 49% HF etch [10] and then dried in a supercritical CO_2 dryer to prevent stiction from destroying the devices. Before bonding the arrays to the oscillator, the Q and series resonant frequency vs bias voltage characteristics of the device were measured in a Lakeshore FWPX vacuum probe station. Arrays of sizes 1, 3, and 5 disks were tested. The single disk dimensional and circuit values and C_0 in Table 3.1 are calculated from the original layout for the devices [10].

Dimension	**Parameter**	**Unit**
Radius	32	um
Thickness	3	um
Coupling Beam	32	um
Gap	80	nm
Anchors	2	
C_m	2.39	aF
L_m	2.93	H
R_m	13k	Ω
C_0	21.5	fF

Table 3.1: Designed dimensions and example circuit parameters of a single 61MHz polysilicon disk at a V_P of $7.45V$.

Afterwards, the resonator was wirebonded to a Pierce oscillator circuit designed and fabricated by Thura Lin Naing [10] and placed into a DIP package. The circuit on the die contains the Pierce circuit and buffer, where the output of the Pierce is only bonded to the buffer to minimize parasitic capacitance. The buffered output signal which can handle

more capacitance then goes off-chip to another buffer to finally drive the cable going into the measurement tools. The entire circuit was placed into a vacuum bulb and pumped down to under 1 millitorr.

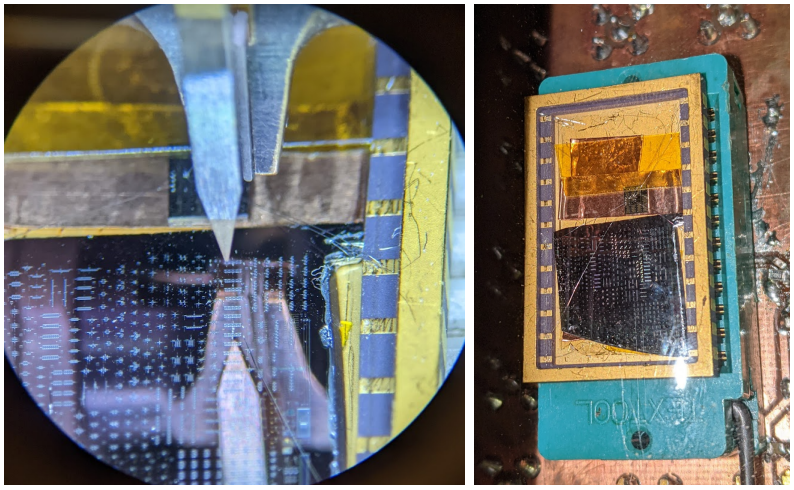

Figure 3.1: Wirebonding process and oscillator circuit in the vacuum bulb.

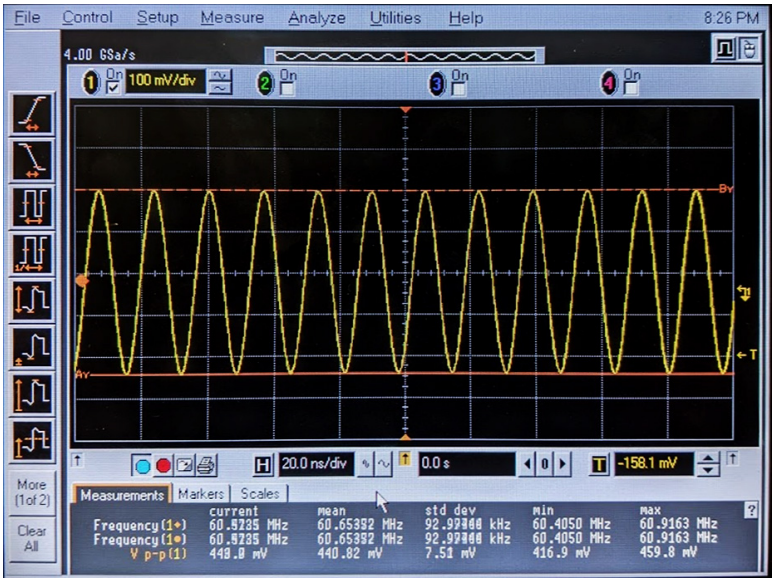

Figure 3.2: Example output waveform from the oscillator.

The phase noise was measured using a HP E5500 Phase Noise Analyzer and the output spectrum was measured on a Agilent N9030A spectrum analyzer. The V_P noise is generated

by a Tektronix AFG3102 signal generator and superimposed on top of the DC voltage with a bias tee.

3.2 Results

The S21 parameters of several of the arrays were collected at varying bias voltages to get the resonant frequency vs bias voltage curves.

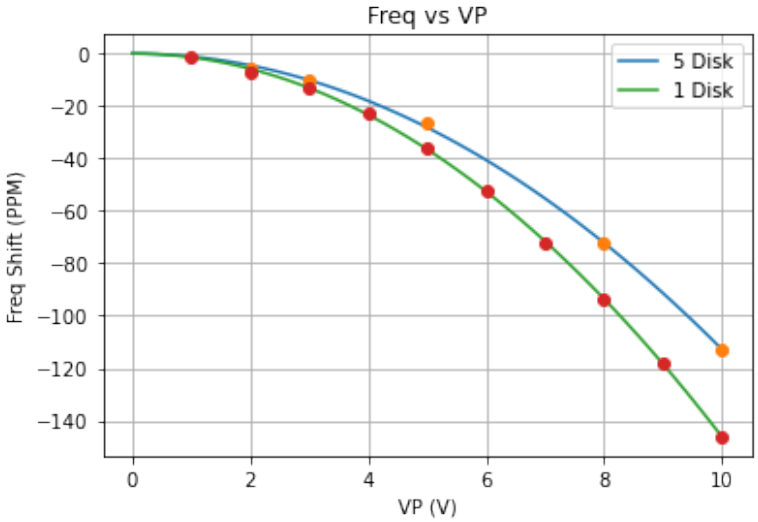

Figure 3.3: Measured resonant frequency vs V_P for 1 and 5 disk arrays.

For the terminations resistance of 50Ω in this measurement the differences in frequency shift between different disk arrays are more than expected from theory. For the amount of frequency change cancellation seen we would expect significantly higher termination resistances, in the order of 10kΩ. This is possibly explained by additional trace and contact resistance that is making the termination resistance higher than expected, along with increasing feedthrough capacitance as the array increases. The Q of the 1 disk resonator was $151k$ and the 5 disk resonator was $60.6k$ at a V_P of 5V.

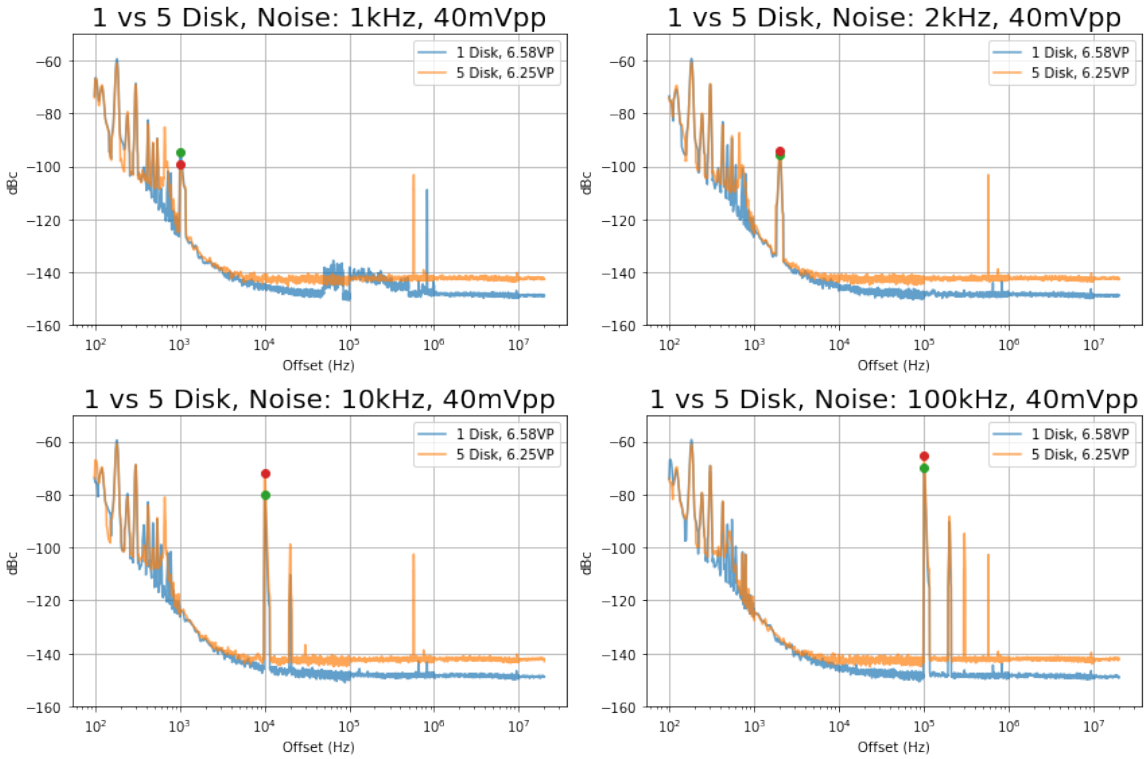

Figure 3.4: Phase noise measurement comparing 1 and 5 disk resonators.

Next, the phase noise of the 1 and 5 disk oscillators were measured with different frequency sinusoid noise signals applied to the bias voltage. The measurement results are presented in Figure 3.4. The absolute level of the spurs is also not comparable between plots at different frequencies due to frequency-dependent attenuation issues with the bias tee used for these measurements, which is described in more detail in the next section. However, we can still measure the difference in spur levels at the same frequency between the array sizes. At 1kHz the red dot shows the 4.2dB improved performance of the 5 disk resonator over the green dot which represents the single disk. This is more than expected from the slope of the frequency vs V_P curve, which predicts 2.7dB. This can be attributed to further increase loading from the wirebonds and circuit parasitics in the IC. One thing to note is that the V_P for the 5 disk array is not $\sqrt{5}$ times smaller than the V_P for a single disk. We were unable to get sustained oscillation at a lower V_P mostly due to the decreased Q of the array compared to a single disk and partially because of increased loading of larger feedthrough capacitance and C_0 for the larger array (as other parasitic capacitances likely still dominate for both 1 and 5 disk arrays). The lower Q is also the cause for the reduced oscillation power and amplitude of the 5 disk array, leading to worse far-from-carrier performance.

This noise measurement outputs a single sided spectrum and as a result we cannot differentiate between the left and right sideband levels. To see the difference, we measured the

oscillators' output spectrums with the spectrum analyzer. Their operating conditions are listed in Table 3.2. The far-from-carrier flat level is higher for the 5 disk due to the decreased power of carrier of the 5 disk oscillation and reduced Q [11] of the the 5 disk resonator.

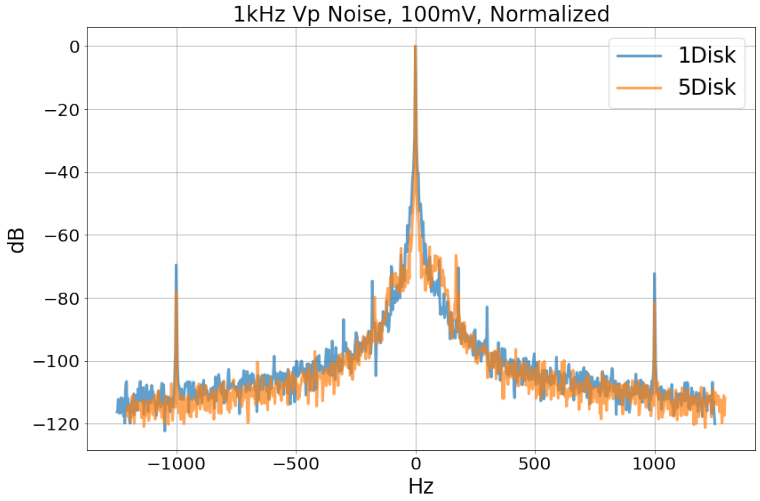

Figure 3.5: Normalized spectrum of 1 and 5 disk resonators during one of the measurements.

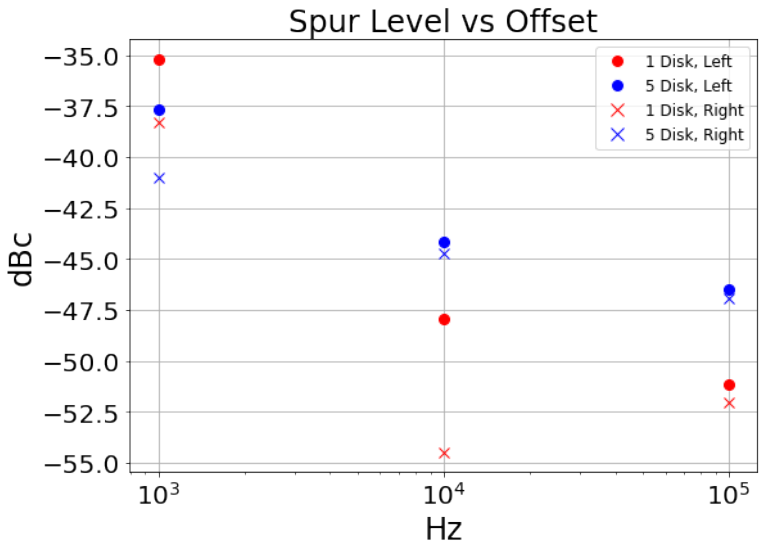

Figure 3.6: Corrected spur level vs offset for 1 and 5 disk resonators from a 40mVpp sinusoid noise source.

Array	V_P	Amplitude (mV)	V_{pierce} (V)	I_{pierce} (uA)	V_{res} (V)
1 Disk	6.1	620	1.8	10	1.1
5 Disk	6.16	495	1.8	10	1.14

Table 3.2: Oscillator bias conditions for Figure 3.6's measurement.

As a result of reduced frequency modulation contributed noise, we can see in Figures 3.5 and 3.6 that the 5 disk oscillator's spectrum is less asymmetric than the 1 disk oscillator. The right side spur has less noise being subtracted from the upper sideband and added to the lower from the FM noise. Close to carrier, where the frequency modulation noise dominates [2], we do indeed see better noise performance with the 5 disk oscillator. We see a 2.5dB improvement at 1kHz with the 5-disk array compared to the 1-disk array, which is in-line with the predicted 2.7dB from the frequency vs V_P curve. We also see a general trend of the spur level decreasing with increasing offset, consistent with the theory and equation (2.24) that the noise will be shaped by the Q of the resonator. As a result the far-from-carrier noise of the 5 disk resonator is also higher than the 1 disk resonator as it had a lower Q and oscillation level, leading to higher off-resonance noise currents relative to the carrier.

This data had a correction factor applied to the levels to account for the attenuation of the noise input by the bias tee which was not designed to operate down to 1kHz. We measured the S_{21} of the bias tee to create the correction factor. This linear increase is valid for us to make at least for small amplitudes where the attenuation was the highest since we tried different levels that led to linear increase in the spur level. Figure 3.7 shows different spur levels for increasing noise amplitudes, and at least for the 1kHz and 10kHz offsets we see a $20\log(x)$ increase as the voltage increases by x times. At 100kHz there is no more attenuation from the bias tee and no correction was applied for those points.

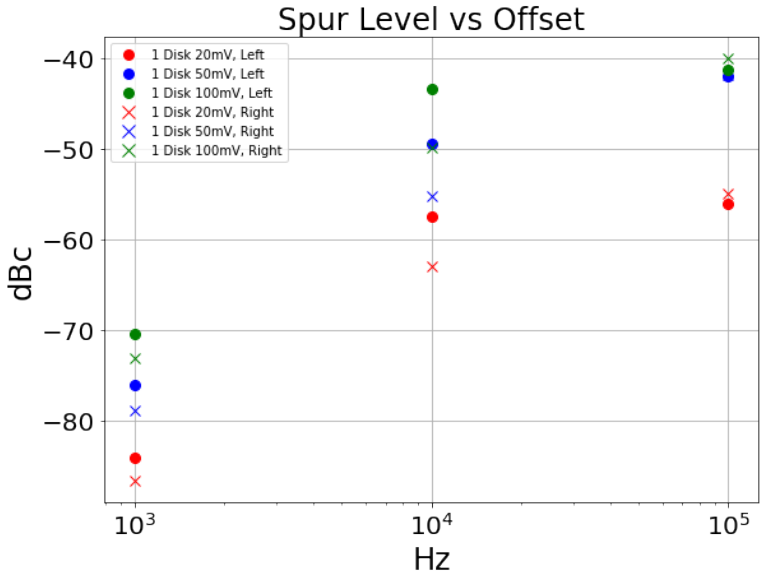

Figure 3.7: Uncorrected spur data for different input noise peak-to-peak voltage levels.

However, there is definitely some limiting of spur levels at higher amplitude noise levels. Noise voltages of 100, 500, and 1000mV peak-to-peak were superimposed onto the bias voltage for a 3 disk oscillator and the spur level increase is no longer linearly increasing with injected noise level. This was also tested across three different bias voltage operating points of 8, 9, and 10V, where the results are summarized in Figure 3.8.

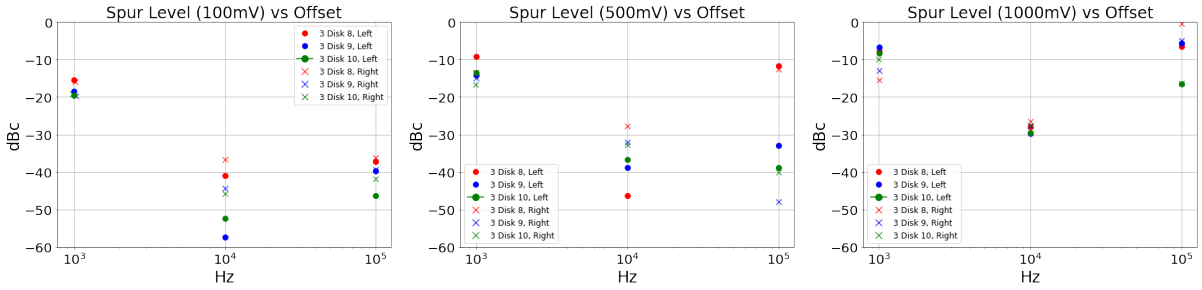

Figure 3.8: Corrected spur data for different input noise peak-to-peak voltage levels.

Unlike the previous data comparing the 1 and 5 disk resonators, the right side spur in all operating conditions in Figure 3.8 is actually higher than the left consistently at the 10kHz and 100kHz offsets. This can also be seen for the 100kHz offset in the 1 disk data in Figure 3.7. This is not what was expected from the frequency modulation noise subtracting on the upper frequency and may be attributed to the FM modulation no longer being in phase

with the amplitude of the driving signal. This inconsistency doesn't seem to follow a trend with respect to the number of disks. The left spur should have additive frequency noise and amplitude noise while the right spur has subtractive frequency noise, and one can see how the left spur is consistently higher in level than the right only at the closest offset.

Our measurements in Figure 3.6 do not show the voltage noise increasing with frequency, as was observed in previous work on a tuning fork resonator [2]. Beyond noise feeding directly through C_0, there is no expectation for the voltage noise to increase with frequency; indeed, Equation 8 in [2] for voltage noise is independent of frequency, making the reference's [2] Figure 8, which does show dependence, somewhat suspect. Instead, our measurements show voltage noise decreasing at higher offsets that is consistent with our analysis that the level is shaped by the Q of the resonator.

Chapter 4

Conclusion

This work demonstrates the improvement in the phase noise of wine-glass mode disk resonator-based oscillators to electrical noise on the main bias voltage by arraying multiple resonators compared to a single resonator. Beyond the improvement in frequency pulling from the increasing feedthrough capacitance associated with more resonators, larger array based oscillators are better than single element ones when running at the same equivalent motional resistance by lowering the V_P by a factor of $\sqrt{N}$ where N is the number of resonators in an array. The tradeoff of using multi-disk arrays for better close-to-carrier noise rejection is potentially worse far-from-carrier rejection. This is due to the decreased Q and increased loading of the real arrayed resonator compared to the single disk resonator, reducing the oscillation level leading to a decreased ratio between the carrier and the off-resonance noise frequency. Increasing the power used by the sustaining circuit for higher amplitudes can improve on this issue. As this work would be most applicable to noise that is injected by a power supply that generates V_P, this shows that if one has a high-frequency switching supply, at the same power level one would ideally want to use smaller array configurations for better far-from-carrier phase noise performance. However, smaller arrays will generally require higher bias voltages to begin with to achieve equivalent motional resistances. One would need to strike a tradeoff between the desired motional resistance of the resonator, the power required by the sustaining circuit and bias generator for that resistance and amount of loading capacitance from the array, and the impact of the noise on the stability of the output frequency. To get the same output level with an array one would need more power in the sustaining circuit.

These experiments also show the need for continued testing across multiple copies of the same resonator to work out the exact relationship of the frequency modulation contributed noise to the output from the input noise. The inversion of the right side spur being higher than the left for the three disk devices that was not seen in the one or five-disk experiments needs more explanation. Future work could consider the bandwidth of the frequency modulation more carefully as the results from these experiments do show spur levels inconsistent with a non-bandwidth limited, perfectly in-phase FM modulation.

Another avenue of investigation would be to measure the performance of larger arrays in

different layout configurations or different sustaining amplifiers. Currently only wine-glass disk resonators are considered in this study and other designs will have different sensitivities to bias voltage noise, especially "widely-tunable" devices intended to have large changes in resonance frequency with changes in V_P. Higher order terms of the electrical stiffness and its nonlinearities could also be analyzed to see how they contribute to the upconversion of the bias voltage noise. Future passive filter design work using these resonator arrays in non-oscillator circuits could also be done with higher termination resistances in mind for better V_P stability.

Bibliography

[1] Alper Ozgurluk. "High-Q Strong Coupling Capacitive-Gap Transduced RF Micromechanical Resonators". PhD thesis. EECS Department, University of California, Berkeley, Jan. 2020. URL: http://www2.eecs.berkeley.edu/Pubs/TechRpts/2020/EECS-2020-6.html.

[2] M. Agarwal et al. "Effects of Mechanical Vibrations and Bias Voltage Noise on Phase Noise of MEMS Resonator Based Oscillators". In: *19th IEEE International Conference on Micro Electro Mechanical Systems*. 2006, pp. 154–157. DOI: 10.1109/MEMSYS.2006.1627759.

[3] Lingqi Wu et al. "Micromechanical disk array for enhanced frequency stability against bias voltage fluctuations". In: *2013 Joint European Frequency and Time Forum International Frequency Control Symposium (EFTF/IFC)*. 2013, pp. 547–550. DOI: 10.1109/EFTF-IFC.2013.6702298.

[4] H.C. Nathanson et al. "The resonant gate transistor". In: *IEEE Transactions on Electron Devices* 14.3 (1967), pp. 117–133. DOI: 10.1109/T-ED.1967.15912.

[5] Mehmet Akgul et al. "A negative-capacitance equivalent circuit model for parallel-plate capacitive-gap-transduced micromechanical resonators". In: *IEEE Transactions on Ultrasonics, Ferroelectrics, and Frequency Control* 61.5 (2014), pp. 849–869. DOI: 10.1109/TUFFC.2014.2976.

[6] E.A. Vittoz. *Low-Power Crystal and MEMS Oscillators: The Experience of Watch Developments*. May 2010. ISBN: 978-90-481-9394-3. DOI: 10.1007/978-90-481-9395-0.

[7] Alper Ozgurluk, Mehmet Akgul, and Clark T.-C. Nguyen. "RF Channel-Select Micromechanical Disk Filters—Part I: Design". In: *IEEE Transactions on Ultrasonics, Ferroelectrics, and Frequency Control* 66.1 (2019), pp. 192–217. DOI: 10.1109/TUFFC.2018.2881727.

[8] Ark-Chew Wong and C.T.-C. Nguyen. "Micromechanical mixer-filters ("mixlers")". In: *Journal of Microelectromechanical Systems* 13.1 (2004), pp. 100–112. DOI: 10.1109/JMEMS.2003.823218.

[9] M.A. Abdelmoneum, M.U. Demirci, and C.T.-C. Nguyen. "Stemless wine-glass-mode disk micromechanical resonators". In: *The Sixteenth Annual International Conference on Micro Electro Mechanical Systems, 2003. MEMS-03 Kyoto. IEEE.* 2003, pp. 698–701. DOI: 10.1109/MEMSYS.2003.1189845.

[10] Thura Lin Naing. "Capacitive-Gap MEMS Resonator-Based Oscillator Systems for Low-Power Signal Processing". PhD thesis. EECS Department, University of California, Berkeley, May 2017. URL: http://www2.eecs.berkeley.edu/Pubs/TechRpts/2017/EECS-2017-14.html.

[11] T.H. Lee and A. Hajimiri. "Oscillator phase noise: a tutorial". In: *IEEE Journal of Solid-State Circuits* 35.3 (2000), pp. 326–336. DOI: 10.1109/4.826814.